




Performance of Quebracho extract as eco-friendly corrosion inhibitor for SAE 1010 steel in the oil field environment

Katryanne R. G. Bacca¹ | Natália F. Lopes¹  | Juliane B. Marcolino¹ |
Fábio dos Santos Grasel²  | Eleani M. da Costa¹ 

¹School of Technology, Materials Laboratory, Pontifical Catholic University of Rio Grande do Sul, Porto Alegre-RS, Brazil

²Dorf Ketal Brazil, Nova Santa Rita, RS, Brazil

Correspondence

Eleani M. da Costa, School of Technology, Pontifical Catholic University of Rio Grande do Sul, 6681 Ipiranga Avenue, Building 30, Room 111/F, Porto Alegre-RS 90619-900, Brazil.

Email: eleani@pucrs.br

Funding information

Coordenação de Aperfeiçoamento de Pessoal de Nível Superior–Brasil (CAPES), Grant/Award Number: Finance Code 001

The inhibitive behavior of Quebracho tannin extract on SAE 1010 steel corrosion in the acidic media is investigated. Potentiodynamic polarization, electrochemical impedance spectroscopy (EIS), and scanning electron microscopy (SEM) are first used to determine the inhibition efficiency of Quebracho in 0.1 M HCl solution to identify the best extract concentration to subsequently evaluate the inhibitor activity in CO₂-rich aqueous solution at high pressure (15 MPa) and high temperature (70°C). Polarization curves revealed that Quebracho extract acted as cathodic inhibitor and that the inhibition efficiency is dependent on the extract concentration. The EIS measurements and SEM analysis showed that the inhibitor had been adsorbed on the steel surface. The inhibition efficiency of Quebracho in CO₂ medium was similar to the 0.1 M HCl, reducing expressively the corrosion rate. The SEM images and X-ray diffraction analysis showed that iron carbonate was the main corrosion product formed on the metal surface in CO₂-rich environment in the presence of Quebracho. Besides, the corrosion scale was thinner and more compact in the presence of inhibitor.

KEYWORDS

CO₂-corrosion, green inhibitor, Quebracho tannin extract

1 | INTRODUCTION

Carbon steels are widely used in oil and gas transportation systems by the petroleum industry. However, this category of steels is very susceptible to corrosion in the oil field environments. The corrosion of material results in the loss of mechanical properties and can cause severe damage in pipelines and equipment, which affects the production due to need of pause for maintenance or replacement of components. Additionally, the corrosion failure can generate disasters with serious consequences to environmental becoming a problem of worldwide significance.^[1–3]

Among the types of corrosion, corrosion of steel by carbon dioxide in aqueous environment is responsible for most of the tasks related to oil and gas fields, having a significant impact on the oil industry.^[1–4] The CO₂ dissolved in water leads to the formation of carbonic acid (H₂CO₃), which dissociates into hydrogen ions (H⁺) and bicarbonate ions (HCO₃[−]). Additionally, bicarbonate ions also dissociate into hydrogen ions (H⁺) and carbonate ions (CO₃^{2−}). When the HCO₃[−] and CO₃^{2−} ions interact with the Fe²⁺ ions, they form iron carbonate (FeCO₃) as main corrosion product, which can attenuate or not the corrosion depending on its properties.^[2,5–8] In case of FeCO₃ formation with protective characteristics, it

performs as a barrier to ionic diffusion on the steel surface promoting a decrease in corrosion rates. However, the FeCO_3 scale when exposed to atmospheres with the presence of oxygen can undergo chemical changes that modify its properties via decomposition into FeO and CO_2 affecting the protection. Besides, the iron oxide may still experience further chemical transformations.^[5,9-14] Choi et al.^[9] observed that the addition of oxygen increased the corrosion rate of the API 5LX65 steel and that the surface of the steel was covered by a porous scale with no defined morphology and when oxygen was present in the corrosive medium the scale basically was composed of oxygen and iron.

Furthermore, acidizing, which is a process used to improve oil production, can also promote corrosion in the production tubing and other components. In this case, the corrosion rates in carbon steels are very high, as acidizing is usually carried out using heated acid solutions. Hot hydrochloric acid at 15–28% is often used for stimulation of the oil well.^[15-19]

Corrosion mitigation in the oil and gas industry has been done by using inhibitors, application of protective coatings, employing cathodic or anodic protection, and by means of adequate corrosion monitoring and inspection. In many cases, the use of inhibitors to corrosion control is more advantageous once the addition of inhibitor substance can be done without suspension of the process. Toxicity, environmental impacts, availability, and cost are some of issues that are considered before choosing a corrosion inhibitor in the oil and gas industry. In general, organic inhibitors have been demonstrating to be more effective for steel corrosion protection in acid media than inorganic compounds. Amines, acetylene alcohols, quaternary ammonium salts, and aldehydes are some of inhibitors used for oil well acidization.^[3,16,20]

The use of different natural extracts as corrosion inhibitors, known as green corrosion inhibitors, is currently being studied because they come from renewable resources, are nontoxic, easily available, and inexpensive. Extracts of vegetables, fruits, woods, seeds, barks, leaves, among others, were tested as corrosion inhibitors for steel in different corrosive media and the results showed that these materials have the potential to be used in corrosion control.^[21-28] The inhibition efficiency increases with extract concentration and usually acts as cathodic or mixed-type inhibitor. The mechanism of metal protection is by adsorption of extract compounds on the metal surface. The inhibition of the corrosive process with the use of natural inhibitors is usually attributed to the presence of tannin that has antioxidant properties due to the polyphenolic compounds and flavonoids present in its molecule. Some studies have shown that the tannin's

performance as corrosion inhibitors is very satisfactory in acidic environments.^[24,27,28]

The Quebracho colorado is a tree from South America found in Argentina, Bolivia, and Paraguay. This plant, popularly known as Quebracho, is divided into two different species, being these *Schinopsis lorentzii* and *Schinopsis balansae*, belonging to the family Anacardiaceae.^[29] Quebracho is known by the high tannin content in its wood, more specifically proanthocyanidins. For extraction of the proanthocyanidins, the wood is chipped and boiled in an aqueous medium. To enhance the extraction of these compounds, sodium bisulfite may be added during boiling. This process decreases proanthocyanidin structures and increases the solubility by the insertion of sulfonic groups. Quebracho extract contains approximately 95% of proanthocyanidins and 5% of water-soluble sugars.^[29-32] Venter et al.^[29] characterized the proanthocyanidins extracted from this plant by electrospray ionization. The authors have found that the predominant structures in these proanthocyanidins are dimers to heptamers, with a catechin starter unit and fisetinidol extender units condensed in the C4–C6 and C4–C8 positions, as shown in the scheme of Figure 1.

Currently, the most important industrial fonts of proanthocyanidins are from Quebracho (*S. balansae* and *S. lorentzii*) and black wattle (*Acacia mearnsii*) bark extracts.^[29,31,33] Among several applications, proanthocyanidins are utilized in leather manufacture, adhesives, purification of water, and to decrease viscosity of drilling mud for oil wells. However, the analysis of performance of these extracts as corrosion inhibitor for steel in oil field environments is not much explored yet.^[17,19,34,35] The

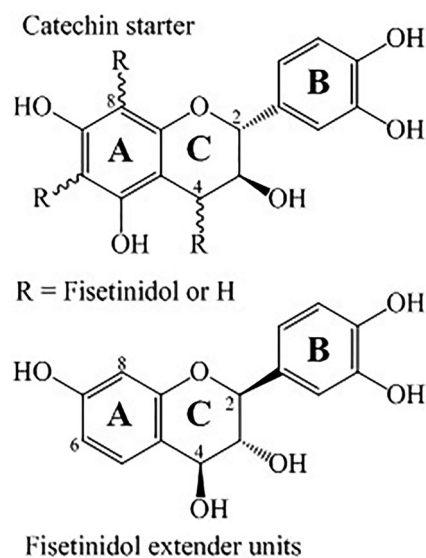


FIGURE 1 General structure of Quebracho proanthocyanidins

literature is particularly scarcely about the investigation of performance of green corrosion inhibitors in CO₂-rich medium, and no information was found in conditions involving tests at high pressures. Thus, the main aim of this study is to investigate the use of the Quebracho tannin extract as an environmentally friendly inhibitor of the corrosion process of SAE 1010 steel in both 0.1 M HCl solution at room temperature and water saturated with CO₂ at high pressure and high temperature.

2 | MATERIALS AND METHODS

2.1 | Materials

Samples of the low carbon steel (SAE 1010) of the pearlite and ferritic microstructure were used in the corrosion tests. Optical emission spectroscopy was used to determine chemical composition of the steel and is presented in Table 1. Before the corrosion tests, the samples were mechanically polished with silicon carbide paper using different grades ($\neq 220$ up to $\neq 1,200$), rinsed with distilled water, and cleaned with acetone.

Quebracho (*S. balansae* and *S. lorentzii*) bark tannin extract (Indusol ATO—cold soluble ordinary Quebracho powder extract) was acquired from Silvateam Brasil Ind. This extract passed by a sulphiting process to transform the phlobaphenes into soluble tannins. According to the producer, this extract has high tannin content ($72 \pm 1.5\%$), while the remaining 28% are composed of 8% humidity and 20% sugar or organic acids, and its pH is 4.7 ± 0.3 in an aqueous solution of 6.9 °Bé. The solutions for the corrosion tests were prepared dissolving Quebracho extract in distilled water using an ultrasonic bath for about 10 minutes to homogenize the solution. The solution in presence of Quebracho is transparent and has a light brownish color.

Spectroscopic analysis of Quebracho was carried out using a PerkinElmer Spectrum 400 model spectrophotometer with Fourier transform infrared spectroscopy. The spectrophotometer is equipped with a DTGS detector and universal attenuated total reflectance accessory (FTIR-UATR). The 3,800–650 cm⁻¹ spectral range, 4 cm⁻¹ resolution, and 32 scans were utilized for analysis. The sample of Quebracho powder was analyzed in the as received condition.

2.2 | Corrosion tests in 0.1 M HCl

First, corrosion inhibition tests were performed in 0.1 M HCl solution at atmospheric pressure and at room temperature by using potentiodynamic polarization (PP) and electrochemical impedance spectroscopy (EIS) techniques aiming to identify the concentration most appropriate to later evaluate the corrosion inhibition activity in CO₂-rich media at high pressure. For this purpose, solutions with different concentrations (0, 0.5, 1.5, and 6 g/L) were prepared with the Quebracho tannin extract.

The electrochemical tests were done using a potentiostat/galvanostat from Autolab, PGSTAT302 N model. Before EIS and PP measurements, the open circuit potential (OCP) was measured for 1 hr to reach a steady-state. For EIS measurements, the frequency was varied from 10,000 to 0.1 Hz, with perturbation amplitude of 10 mV. The PP curves were obtained with a scanning rate of 1 mV/s in the range of potential of ± 300 mV in relation to the obtained value of OCP. The electrochemical cell used in the corrosion tests is composed of platinum counter electrode (CE), a saturated calomel reference electrode (SCE), and the steel sample as working electrode (WE) with exposed area of approximately 1 cm². All electrochemical measurements were done in duplicate. The electrochemical parameters were obtained from polarization curves by the Tafel extrapolation method and the electrical parameters were obtained from EIS by fitting using the ZView software, version 2.90 (Scribner Associates, Inc.). Each potential in this study is referred to the SCE ($E = +241$ mV SHE) and the measurements were performed in naturally aerated and unstirred solutions.

Equation (1) was used to calculate the inhibition efficiency E (%) as obtained by the PP technique:

$$E (\%) = \frac{(R_{p_0} - R_{p_i})}{R_{p_i}} \times 100, \quad (1)$$

where R_{p_0} and R_{p_i} are polarization resistance of SAE 1010 steel in 0.1 M HCl without and with inhibitor, respectively.

At the end of each corrosion test, the specimens were washed with distilled water, dried and conserved in a desiccator for further analysis of corroded surfaces using scanning electron microscopy by field emission gun (SEM-FEG).

TABLE 1 Chemical composition (% in weight) of SAE 1010 steel

C	Si	Mn	P	S	Cr	Ni	Al	Co	Cu	Fe
0.118	0.01	0.52	0.012	0.009	0.01	0.01	0.052	0.003	0.009	99.21

2.3 | Corrosion tests in CO₂-saturated water at high pressure and high temperature

The high-pressure corrosion tests simulating an environment similar to that found in oil fields were carried out under static conditions (without flux) in a stainless steel autoclave (Parr Instrument). The corrosion tests were executed in presence of oxygen and with a solution containing 1.5 g/L of Quebracho extract, which was the concentration that allowed the highest inhibition efficiency in 0.1 M HCl medium. For comparison, a corrosion test without using inhibitor was also done in the same experimental conditions. The aqueous solutions with and without Quebracho extract were saturated with carbon dioxide (CO₂) with 99.99% of purity. The temperature and pressure used in the experiments were 70°C and 15 MPa, respectively. The SAE 1010 samples with approximate dimensions of (10 × 10 × 19 mm) and prismatic shape were immersed in the corrosion medium during 168 hr (7 days).

Owing to the difficulty of monitoring the corrosion in situ by electrochemical techniques because of high pressure involved, information about the corrosion inhibition were obtained from mass loss tests and the characterization of the corrosion products formed on the steel surface. Once completed the period of corrosion, the specimens were removed from the autoclave, washed with distilled water, dried, and maintained in a desiccator for posterior characterization.

Tests of mass loss were executed following ASTM G1-90-Standard practice for preparing, cleaning, and evaluating corrosion on test specimens.^[36] The removal of corrosion scale from corroded surface was done by specimen immersion in acid solution at room temperature. The etching solution (1,000 mL) was prepared using HCl and distilled water at 1:1 proportion with addition of 3.5 g hexamethylenetetramine. The time of immersion of each specimen in acid solution was about 30 s and after that, the specimen was immediately washed in distilled water and acetone, dried, and weighted on a balance of 0.0001 g precision. This process was repeated 20 times to obtain the mass loss curves. The corrosion rate (CR) was determined by Equation (2). The tests were done in duplicate for each experimental condition and the corrosion rate values were expressed as average.

$$CR = \frac{K \cdot \Delta w}{A \cdot t \cdot d}, \quad (2)$$

where K is a constant (8.76×10^4 for mm/year), Δw is loss of weight in grams, A is the sample surface area in cm² (9.6 cm²), t is the corrosion exposure time in hours, and d is density of carbon steel (7.86 g/cm³).

The inhibition efficiency (η) of Quebracho extract as corrosion inhibitor was calculated by using the following equation.

$$\eta (\%) = \frac{CR_o - CR_i}{CR_o} \times 100, \quad (3)$$

where CR_o is the corrosion rate without inhibitor and CR_i is the corrosion rate with inhibitor as obtained by mass loss test.

The morphology and thickness of corrosion scales were observed by SEM/FEG. The composition of the corrosion scales was obtained by X-ray diffraction (XRD) using a diffractometer with a Cu K α X-ray source, 40 kV and 30 mA, 0.1542 nm wavelength.

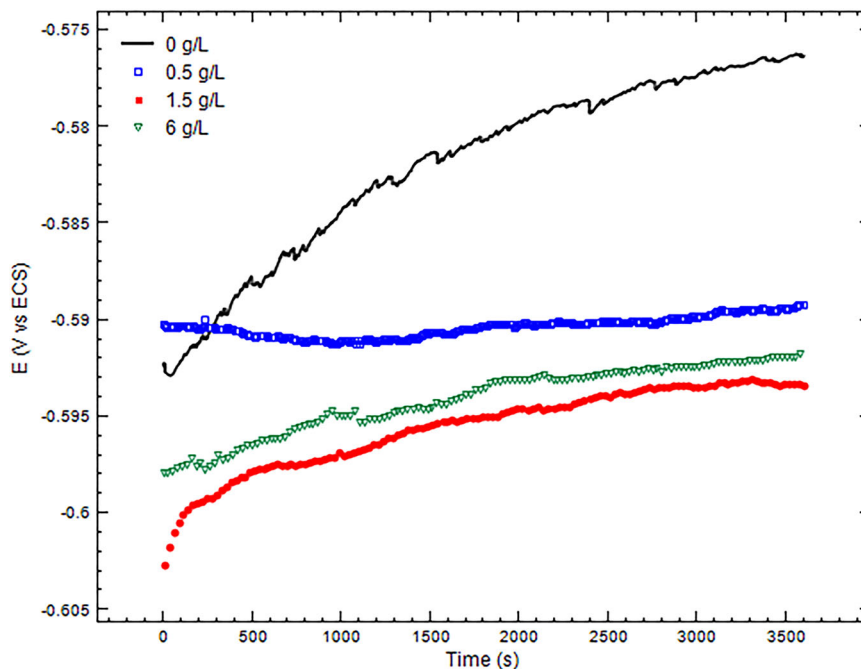
3 | RESULTS AND DISCUSSION

3.1 | Inhibitor performance in 0.1 M HCl medium

Figures 2 and 3 show the OCP plot and the polarization curves, respectively, for SAE 1010 steel for different concentrations of Quebracho extract in 0.1 M HCl solution. Table 2 shows the electrochemical parameters as obtained from the polarization curves by the Tafel extrapolation method, and the inhibition efficiencies were calculated by Equation (1).

It can be observed in the OCP curves (Figure 2) that the presence of Quebracho in solution shifts the potential to more active values and promotes a better stabilization of the OCP with the exposure time to the corrosion medium. The shift of corrosion potential was dependent on the Quebracho concentration. It was also observed in polarization curves (Figure 3) that the presence of Quebracho leads to a reduction in the corrosion current density of both anodic and cathodic branches. However, it can be noted that its action is more accentuated in cathodic reactions (reduction of hydrogen) with a little shift to more active corrosion potential, behaving as a slightly cathodic inhibitor for SAE 1010 steel in 0.1 M of HCl, as also observed by Gerengi and Sahin.^[22] It can be observed in Table 1 that up to 1.5 g/L the current density decreases and the polarization resistance increases with increasing Quebracho concentration. However, at high concentration (6 g/L) the corrosion current density increased in relation to the concentration of 1.5 g/L and the polarization resistance also decreased. The higher polarization resistance obtained with inhibitor addition is an indicative that a nonconducting physical barrier is probably created at the interface of metal and electrolyte.

FIGURE 2 Open circuit potential plots for SAE 1010 steel in 0.1 M HCl solution for different concentrations of Quebracho extract [Color figure can be viewed at wileyonlinelibrary.com]



The corrosion inhibition effect by Quebracho is related with the fact of tannins in aqueous solutions forming insoluble complexes (amorphous ferric-tannates), due to reaction between iron oxide and tannin, which polymerize on the metal surface forming a layer that could act as a physical barrier for mass and transfer charge. The highest inhibition efficiency was obtained for 1.5 g/L of Quebracho with a value of 79%, according to Table 2. The fact that for high concentration of extract (6 g/L) did not provide higher inhibition efficiency can be related to formation of porous layer or weak adsorption

of inhibitor causing secondary desorption from the metal surface, as also observed by Rahim et al.^[28]

EIS measurements after 1 hr of immersion were applied to obtain information about properties of the surface in the presence or absence of inhibitor to help to elucidate the inhibition mechanism.

Figure 4 shows Nyquist diagrams of SAE 1010 steel in 0.1 M HCl solution with different concentrations of the Quebracho extract. It can be seen that for all samples, with and without inhibitor, a single capacitive arc and a small inductive loop are present. The addition of

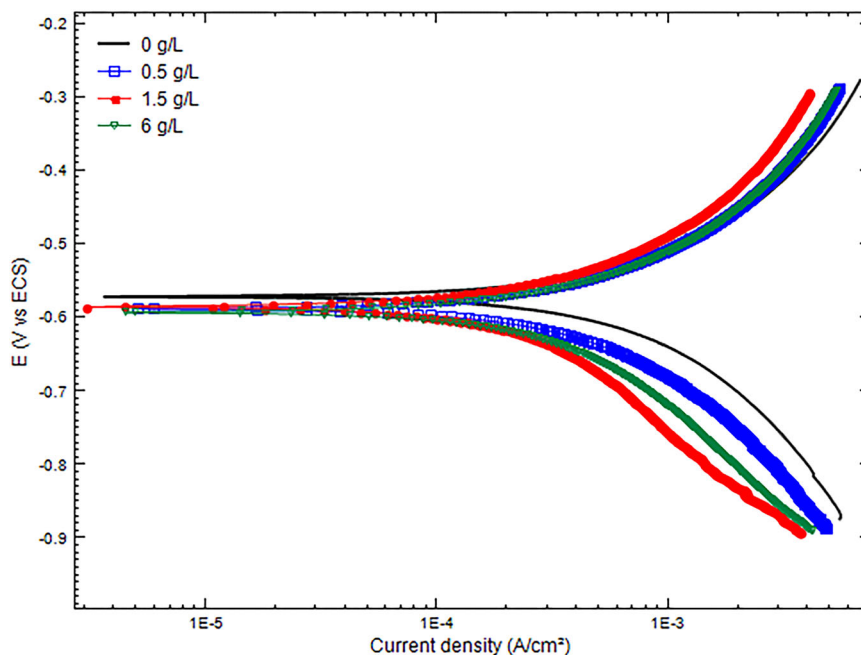


FIGURE 3 Polarization curves for SAE 1010 steel in 0.1 M HCl solution for different concentrations of Quebracho extract [Color figure can be viewed at wileyonlinelibrary.com]

TABLE 2 Potentiodynamic polarization parameters obtained for SAE 1010 steel in 0.1 M HCl with different concentrations of Quebracho extract

Inhibitor concentration (g/L)	E_{corr} (mV)	I_{corr} ($\mu\text{A}/\text{cm}^2$)	Polarization resistance ($\Omega\cdot\text{cm}^2$)	Efficiency (E, %)
0	-570	63	95	-
0.5	-587	54	135	29
1.5	-585	16	451	79
6.0	-592	36	153	38

inhibitor does not change the shape of Nyquist plots, which suggests that steel dissolution mechanism is not altered in presence of inhibitor, as also observed on the PP curves (Figure 3). However, the capacitive arc diameter is dependent on the concentration of Quebracho extract due to changes of resistance, suggesting that the corrosion of SAE 1010 steel is predominantly driven by charge transfer process and adsorption of layer that protects the steel surface. However, the diameter of capacitive arc of 1.5 and 6.0 g/L are almost the same, indicating that there is an optimum concentration of extract to be used. The adsorption of inhibitor molecules on the steel surface can cause replacement of water molecules and adsorbed ions from the surface, decreasing its electrical capacity. The relaxation of adsorbed intermediate species (H^+ , Cl^- , O^{2-} , or inhibitor species) from the steel surface due to corrosion process can be responsible for the inductive behavior observed at low frequency. Several authors^[37-39] have reported this phenomenon of inductive loop at low frequencies. In fact, inductive compartment at low frequency is more evident for high Quebracho content.

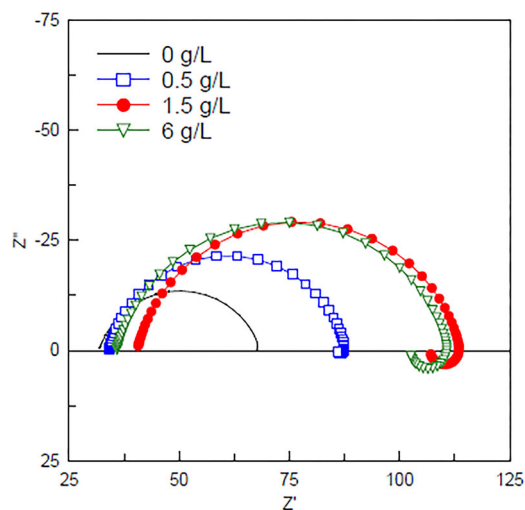


FIGURE 4 Nyquist plot of SAE 1010 steel for different concentrations of the Quebracho extract in 0.1 M HCl solution [Color figure can be viewed at wileyonlinelibrary.com]

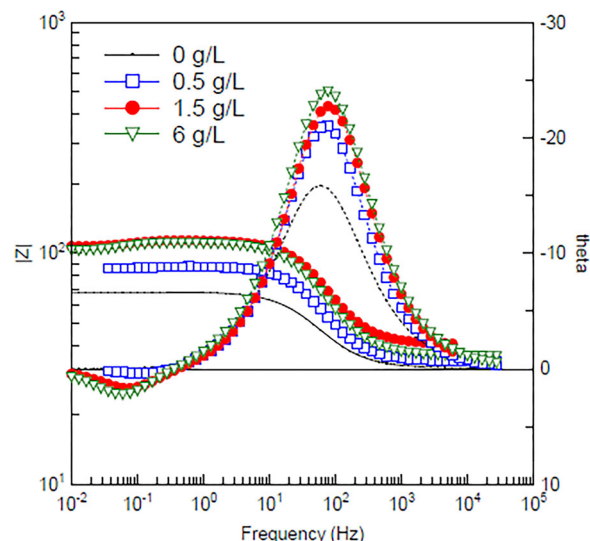


FIGURE 5 Bode modulus and frequency phase-angle plots of SAE 1010 steel for different concentrations of Quebracho extract in 0.1 M HCl solution [Color figure can be viewed at wileyonlinelibrary.com]

The Bode-phase diagrams (Figure 5) show only one capacitive time constant and evidenced that both the impedance modulus $|Z|$ and the phase angle increase with inhibitor concentration, as the adsorption of inhibitor on the steel surface is intensified.

All the diagrams converged very well to the equivalent electric circuit proposed in Figure 6. In the electrical circuit, R_1 is the solution resistance, R_2 the charge transfer resistance, CPE1 the constant phase element, and the inductive elements are R_3 and L . The corresponding electrical results are shown in Table 3. It can be observed in Table 3 that the charge transfer resistance (R_2) increases with inhibitor concentration confirming that the corrosion process is charge-transfer controlled. In addition, the constant phase element (CPE1) decreases in presence of inhibitor reinforcing that the improvement of protection is reached by adsorption of inhibitor molecules on the surface blocking the electrochemical active sites.

The SEM images (Figure 7) confirm that the presence of Quebracho in solution protects the surface of SAE 1010 steel by adsorption inhibitor molecules. In the micrographs of Figure 7a,b corresponding to 0 and 0.5 g/L of inhibitor, respectively, the preferential ferrite dissolution is clearly visible and no deposit on the surface was observed. Furthermore, it can be seen small islands probably

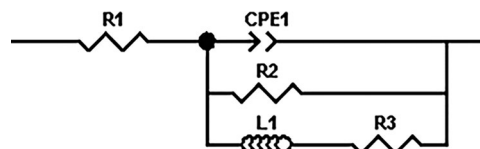


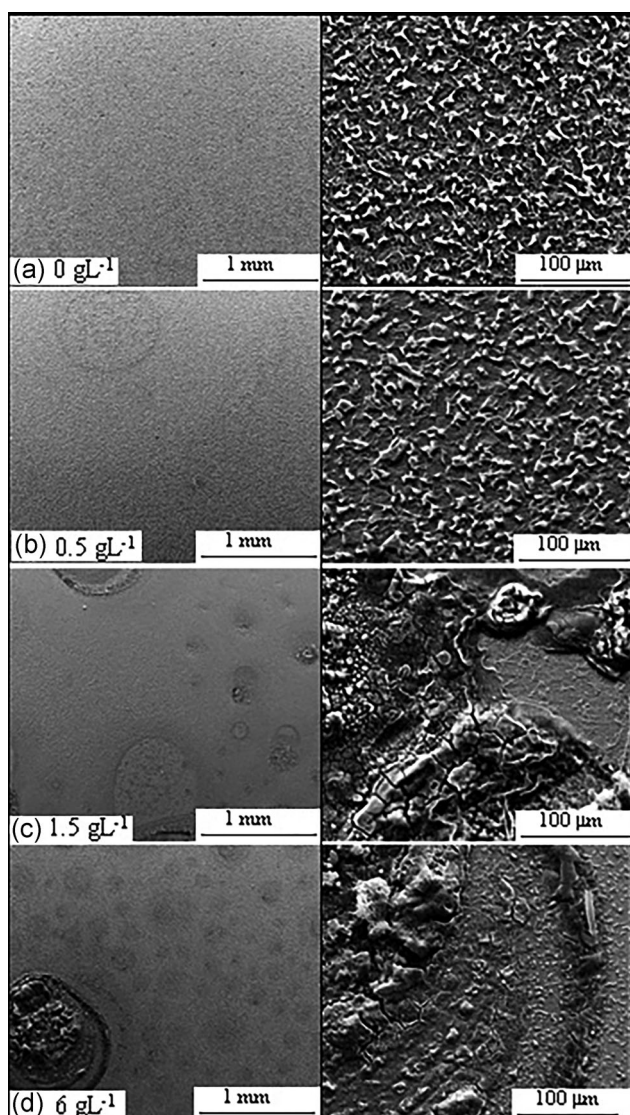
FIGURE 6 Equivalent electric circuit proposed

TABLE 3 Impedance parameters for corrosion of SAE 1010 steel in the absence and presence of different concentrations of the Quebracho extract in 0.1 M HCl solution

Inhibitor concentration (g/L)	χ^2	R1 (Ω)	CPE1 ($\mu\text{F}/\text{cm}^2$)	n	R2 (Ω/cm^2)	L1 (H/cm ²)	R3 (Ω/cm^2)
0	3.96×10^{-4}	31.83	330	0.81	36.63	643.8	1,593
0.5	5.96×10^{-4}	34.04	160	0.86	53.79	1,683	1,226
1.5	3.06×10^{-4}	40.40	113	0.85	73.63	1,683	700.5
6.0	9.61×10^{-4}	35.78	137	0.83	75.56	1,562	562.3

associated to ferric-tannates deposits adsorbed on surface, which are evident when 1.5 and 6 g/L of inhibitor were used (Figure 7c,d).

The FTIR results for the Quebracho are shown in Figure 8 and Table 4. In the analysis of the FTIR spectrum

**FIGURE 7** Scanning electron microscopy images of corroded surface of SAE 1010 steel for different concentrations of the Quebracho extract in 0.1 M HCl solution (a) 0 gL⁻¹(b) 0.5 gL⁻¹(c) 1.5 gL⁻¹(d) 6 gL⁻¹

(Figure 8), a broad band in the region of 3,227 cm⁻¹, can be observed, assigned to -OH stretching and at 2,962 and 2,920 cm⁻¹, the CH, CH₂, and CH₃ stretching vibrations, derived from carbohydrates, sugars, and proanthocyanidin C-ring.^[40] The aromatic bond stretching (C=C-C) appears in the region of 1,605; 1,515; and 1,443 cm⁻¹ and the C-O bond stretching of pyran, typical of proanthocyanidin C-rings, at the 1,358 and 1,286 cm⁻¹.^[40-43] Another C-O bond stretching appears in the region of 1,196-973 cm⁻¹. At 1,117 and 1,087 cm⁻¹ appears the aromatic C-H in plane and at 840, 810, and 771 aromatic C-H out-of-plane bend.^[41-43] The mechanism of metal protection by the Quebracho tannin extract is principally because of the OH⁻ groups on the vicinity of aromatic rings that form chelates with iron ions.^[22]

3.2 | Inhibitor performance in CO₂-saturated water at high pressure and high temperature

The performance of the Quebracho extract was also evaluated in the CO₂-saturated water at high pressure (15 MPa) and high temperature (75°C) using 1.5 g/L, which was the concentration that exhibited the highest inhibition efficiency (79%) in the HCl medium.

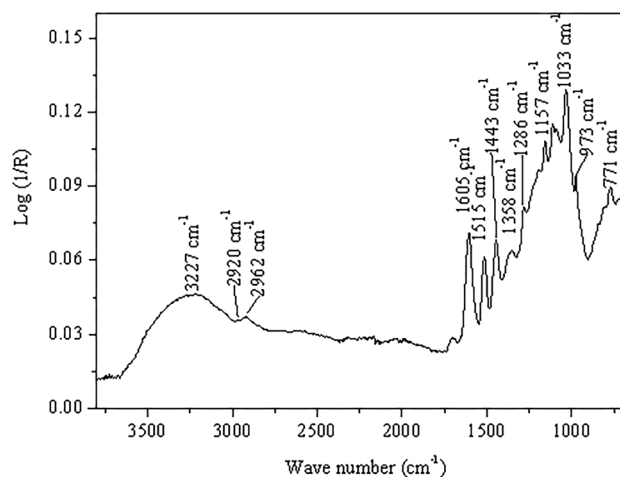
**FIGURE 8** Fourier transform infrared spectroscopy-universal attenuated total reflectance accessory spectrum of Quebracho extract

TABLE 4 Functional groups and frequency assignments for Quebracho extract from the Fourier transform infrared spectroscopy–universal attenuated total reflectance spectrum

Vibrational bands of Quebracho extract		
Vibrational group	Quebracho	Assignment
C–H	771 (m)	Aromatic C–H out-of-plane bend
	810 (w)	
	840 (w)	
C–H	1,087 (w)	Aromatic C–H in plane bend
	1,111 (m)	
C–O	973 (m)	C–O stretch
	1,033 (vs)	
	1,157 (s)	
	1,196 (w)	
	1,286 (w)	
	1,358 (m)	
C=C–C	1,443 (s)	Aromatic ring stretch
	1,515 (m)	
	1,605 (s)	
–CH	2,920 (w)	–CH, –CH ₂ , and –CH ₃ stretch
	2,962 (m)	
–OH	3,227 (vs)	–OH stretch

Abbreviations: m, medium; s, strong; vs, very strong; w, weak.

Figure 9 shows the mass loss curves of SAE 1010 steel corroded in the CO₂-saturated water medium containing 0 and 1.5 g/L of the Quebracho extract at 15 MPa and 70°C. The average corrosion rate calculated by Equation

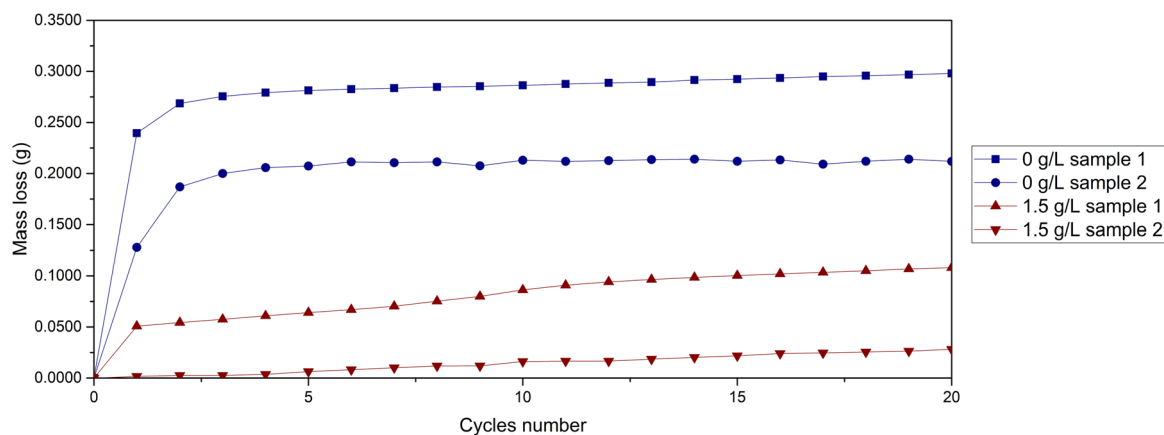


FIGURE 9 Mass loss curves of SAE 1010 steel corroded in CO₂-saturated water medium containing 0 and 1.5 g/L of Quebracho extract at 15 MPa and 70°C [Color figure can be viewed at wileyonlinelibrary.com]

(2) in the absence of inhibitor was 1.639 mm/year and with 1.5 g/L of inhibitor the corrosion rate decreased considerably to 0.395 mm/year, corresponding to an efficiency of inhibition of 76%. This efficiency is very similar to the one obtained when the same concentration of inhibitor in 0.1 M HCl medium was used which was 79%. The scales formed in absence of inhibitor were removed in the second cycle of immersion, whereas in the presence of inhibitor the scales were completely removed only after the tenth cycle suggesting a better adhesion to the steel surface.

Figure 10 shows SEM images of the steel surface after corrosion in CO₂-saturated water medium at 70°C and 15 MPa pressure with and without inhibitor. It is interesting to note that the morphology of corrosion scale is distinct with and without inhibitor. It can be observed that in presence of inhibitor the entire surface of the steel is covered by crystals of iron carbonate (FeCO₃). The iron carbonate crystals have morphological characteristics similar to those formed in the absence of oxygen,^[5,6,9] indicating that the presence of Quebracho avoid the FeCO₃ chemical degradation via reaction with oxygen. Figure 11 presents the cross-section of scales, showing that the scale corresponding to the sample corroded in presence of inhibitor is thinner and more compact when compared with the one formed in the absence of inhibitor. These results suggest that the presence of Quebracho as an inhibitor in the solution leads to the formation of scales with superior protective properties, reducing the corrosion rate.

The XRD was performed to confirm the composition of the scales (Figure 12). Goethite (α -FeOOH) and iron oxides (Fe₃O₄) such as hematite are present in the scale formed without the inhibitor. However, it can be noted that in presence of inhibitor the majority of the peaks is

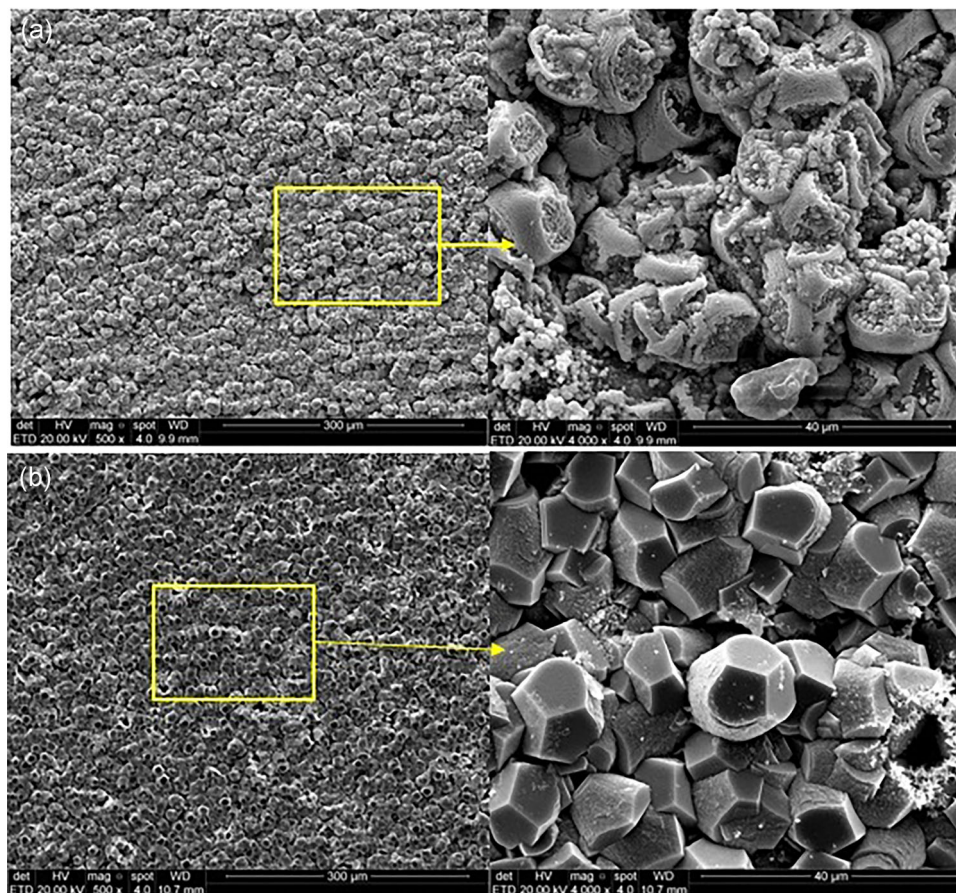


FIGURE 10 Scanning electron microscopy images of the corrosion scales formed on the surface of SAE 1010 steel corroded in CO_2 -saturated water medium at 15 MPa and 70°C during 7 days in the absence of Quebracho extract (a) and in the presence of 1.5 g/L of Quebracho extract (b) [Color figure can be viewed at wileyonlinelibrary.com]

characteristic of FeCO_3 . These results confirm that the presence of Quebracho was effective, preventing the iron carbonate scale from undergoing chemical changes through reaction with oxygen that could compromise its protective characteristics.

The results obtained by SEM and XRD indicate that in absence of inhibitor formation of FeOOH occurs, which results from oxidation of iron metal into ferrous ions (Fe^{2+}) that further is oxidized into ferric ions (Fe^{3+}). Furthermore, the Fe^{3+} in equilibrium with FeOOH can

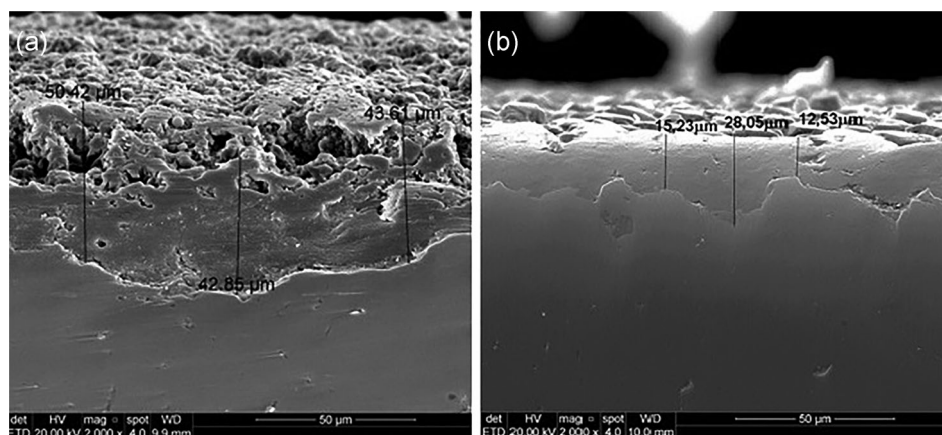


FIGURE 11 Scanning electron microscopy images of cross-section of scales formed on the surface of SAE 1010 steel corroded in CO_2 -saturated water medium at 15 MPa and 70°C during 7 days in the absence of Quebracho extract (a) and in the presence of 1.5 g/L of Quebracho extract (b)

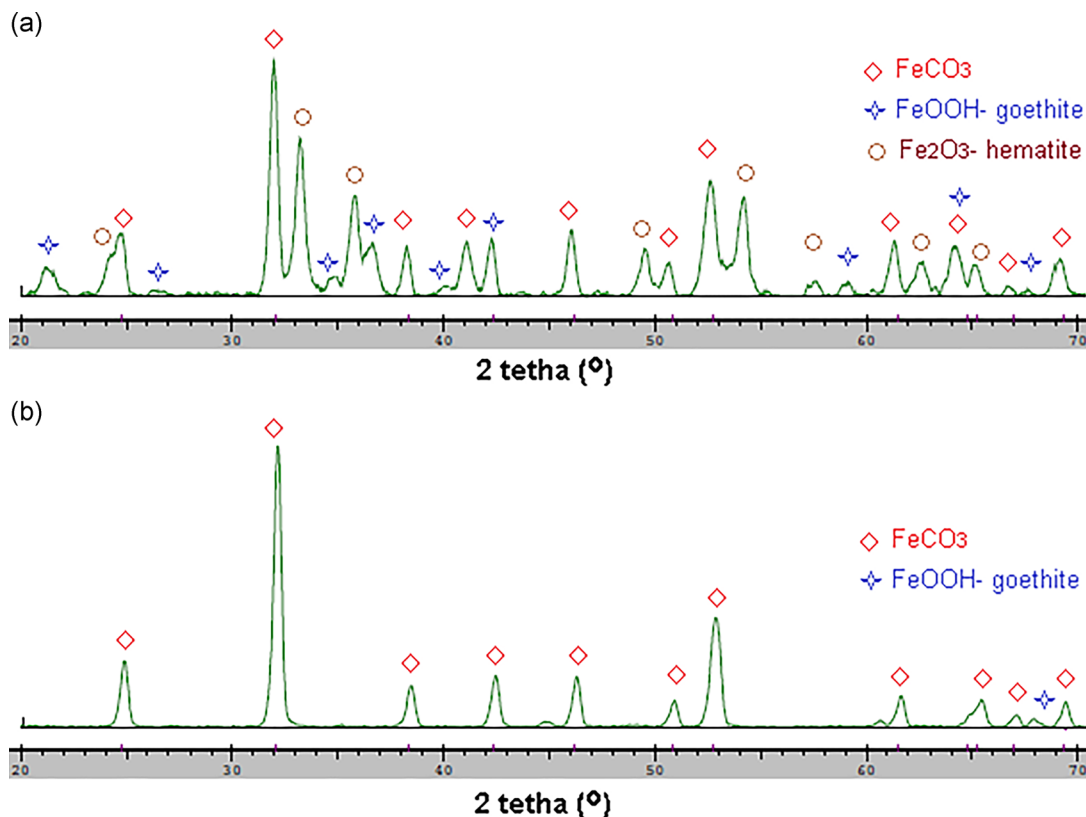


FIGURE 12 X-ray diffraction patterns of scales formed on the surface of SAE 1010 steel corroded in CO_2 -saturated water medium at 15 MPa and 70°C in the absence of Quebracho extract (a) and in the presence of 1.5 g/L of Quebracho extract (b) [Color figure can be viewed at wileyonlinelibrary.com]

be reduced to Fe^{2+} ions due to contact with steel through the pores of the scale, and afterward the Fe^{2+} compounds can be oxidized again forming iron oxides, as previously reported by Stratmann^[44] and Rahim et al.^[28] However, in presence of inhibitor, the tannin molecules may complex with Fe^{2+} ions producing ferrous-tannates, which can also be oxidized into ferric-tannates. In addition, ferric-tannates can be also formed by reacting directly with Fe^{3+} ions; and because of the tannin, high reducing power the Fe(III) oxides can be reduced into Fe^{2+} ions. In the presence of oxygen, the Fe^{2+} ions can then be complexed by tannins forming ferric-tannates.^[24,28,45] Nevertheless, tannate deposits were not observed on the steel surface.

4 | CONCLUSIONS

- The Quebracho extract demonstrated good performance as inhibitor for the SAE 1010 protection in 0.1 M HCl solution and in the oil field environment.
- The polarization curves showed that the Quebracho extract acts predominantly as cathodic inhibitor for corrosion of low carbon steel in 0.1 M HCl medium.


- The EIS measurements and SEM analysis revealed that the corrosion of SAE 1010 steel in 0.1 M HCl is principally controlled by charge transfer process and adsorption of layer that protects the steel surface.
- In water saturated with CO_2 , Quebracho promoted the growth of a thinner and more compact corrosion scale on SAE 1010 steel composed of FeCO_3 , evidencing that it provides favorable conditions for the formation of scale with protective properties in the presence of O_2 .
- The inhibition efficiency of Quebracho in the CO_2 medium was similar to the 0.1 M HCl, reducing expressively the corrosion rate.

ACKNOWLEDGMENTS

The authors acknowledge the support provided by CNPq (The Brazilian Research Council) and Instituto do Petróleo e Recursos Naturais (IPR). This study was financed, in part, by the Coordenação de Aperfeiçoamento de Pessoal de Nível Superior–Brasil (CAPES)—Finance Code 001.

ORCID

Natália F. Lopes  <http://orcid.org/0000-0002-8164-6692>

Fábio dos Santos Grasel  <http://orcid.org/0000-0002-1380-0731>

Eleani M. da Costa  <http://orcid.org/0000-0001-8733-3083>

REFERENCES

- [1] M. Javidi, S. Bekhrad, *Eng. Fail. Anal.* **2018**, *89*, 46.
- [2] D. A. López, T. Pérez, S. N. Simison, *Mater. Des.* **2003**, *24*, 561.
- [3] L. T. Popoola, S. G. Alhaji, K. L. Ganiyu, G. Babagana, S. B. Adebiori, *Int. J. Ind. Chem.* **2013**, *4*.
- [4] Y. Zhang, X. Pang, S. Qu, X. Li, K. Gao, *Corros. Sci.* **2012**, *59*, 186.
- [5] R. A. De motte, R. Barker, D. Burkle, S. M. Vargas, A. Neville, *Mater. Chem. Phys.* **2018**, *216*, 102.
- [6] L. M. Tavares, E. M. Costa, J. J. O. Andrade, R. Hubler, B. Huet, *Appl. Surf. Sci.* **2015**, *359*, 143.
- [7] J. Zhao, D. Xiong, Y. Gu, Q. Zeng, B. Tian, *J. Petrol. Sci. Eng.* **2019**, *173*, 1109.
- [8] Z. F. Yin, W. Z. Zhao, Y. R. Feng, Y. H. Li, C. X. Yin, *Mater. Corros.* **2009**, *60*, 5.
- [9] Y. S. Choi, S. Nestic, D. Young, *Environ. Sci. Technol.* **2010**, *44*, 9233.
- [10] J. K. Heuer, J. F. Stubbins, *Corros. Sci.* **1999**, *41*, 1231.
- [11] Y. Hua, R. Jonnalagadda, L. Zhang, A. Neville, R. Barker, *Int. J. Greenh. Gas Control.* **2017**, *64*, 126.
- [12] T. Li, Y. Yang, K. Gao, M. Lu, *J. Univ. Sci. Technol. B* **2008**, *15*, 702.
- [13] C. Sun, J. Sun, Y. Wang, P. Sui, X. Lin, H. Liu, X. Cheng, M. Zhou, *Int. J. Greenh. Gas Control* **2017**, *65*, 117.
- [14] X. Zhong, W. Lu, H. Yang, M. Liu, Y. Zhang, H. Liu, J. Hu, Z. Zhang, D. Zeng, *J. Petrol. Sci. Eng.* **2019**, *172*, 162.
- [15] K. R. Ansari, M. A. Quraishi, A. Singh, *J. Assoc. Arab. Univ. Bas. App. Sci.* **2017**, *22*, 45.
- [16] S. Aribio, S. J. Olusegun, L. J. Ibhadiyi, A. Oyetunji, D. O. Folorunso, *J. Assoc. Arab. Univ. Bas. App. Sci.* **2017**, *24*, 34.
- [17] K. Haruna, I. B. Obot, N. K. Ankah, A. A. Sorour, T. A. Saleh, *J. Mol. Liq.* **2018**, *264*, 515.
- [18] P. Parthipan, J. Narenkumar, P. Elumalai, P. S. Preethi, A. Usha Raja Nanthini, A. Agrawal, A. Rajasekar, *J. Mol. Liq.* **2017**, *240*, 121.
- [19] M. Soudani, M. H. Meliani, K. El-Miloudi, Z. Azari, A. A. Sorour, N. Merah, G. Pluvinage, *Int. J. Hydrog. Energy* **2018**, *43*, 11150.
- [20] A. A. Olajire, *J. Mol. Liq.* **2017**, *248*, 775.
- [21] S. Banerjee, V. Srivastava, M. M. Singh, *Corros. Sci.* **2012**, *59*, 35.
- [22] H. Gerengi, H. I. Sahin, *Ind. Eng. Chem. Res.* **2012**, *51*, 780.
- [23] L. A. L. Guedes, K. G. Bacca, N. F. Lopes, E. M. Da Costa, *Mater. Corros.* **2019**, doi.org/10.1002/maco.201810667.
- [24] A. A. Rahim, E. Rocca, J. Steinmetz, M. Jain Kassim, *Corros. Sci.* **2008**, *50*, 1546.
- [25] P. B. Raja, M. G. Sethuraman, *Mat. Lett.* **2008**, *62*, 113.
- [26] C. Verma, E. E. Ebenso, I. Bahadur, M. A. Quraishi, *J. Mol. Liq.* **2018**, *266*, 577.
- [27] R. S. Peres, E. Cassel, D. S. Azambuja, *ISRN Corros.* **2012**, *2012*, 1.
- [28] A. A. Rahim, E. Rocca, J. Steinmetz, M. J. Kassim, R. Adnan, M. Sani Ibrahim, *Corros. Sci.* **2007**, *49*, 402.
- [29] P. B. Venter, N. D. Senekal, M. Amra-Jordaan, S. L. Bonnet, J. H. Van der Westhuizen, *Photochemistry* **2012**, *78*, 156.
- [30] D. Fengel, Holzforschung, *Int. J. Biol. Chem. Phys. Tech. Wood.* **1991**, *45*, 259.
- [31] P. B. Venter, M. Sisa, M. J. van der Merwe, S. L. Bonnet, J. H. van der Westhuizen, *Photochemistry* **2012**, *73*, 95.
- [32] D. G. Reid, S. L. Bonnet, G. Kemp, J. H. van der Westhuizen, *Phytochemistry* **2013**, *94*, 243.
- [33] F. S. Grasel, M. F. Ferrão, *Anal. Methods* **2018**, *10*, 968.
- [34] G. Cui, J. Guo, Y. Zhang, Q. Zhao, S. Fu, T. Han, S. Zhang, Y. Wu, *Carbohydr. Polym.* **2019**, *203*, 386.
- [35] B. J. Usman, S. A. Umoren, Z. M. Gasem, *J. Mol. Liq.* **2017**, *237*, 146.
- [36] ASTM G1-90, *Standard Practice for Preparing, Cleaning, and Evaluating Corrosion Test Specimens*, ASTM International, West Conshohocken, PA **1999**.
- [37] I. V. Aoki, I. C. Guedes, S. L. A. Maranhão, *J. Appl. Electrochem.* **2002**, *32*, 915.
- [38] P. Singh, M. Makowska-Janusik, P. Slovensky, M. A. Quraishi, *J. Mol. Liq.* **2016**, *220*, 71.
- [39] N. A. Odewunmi, S. A. Umoren, Z. M. Gasem, *J. Ind. Eng. Chem.* **2015**, *21*, 239.
- [40] A. Ricci, K. J. Olejar, G. P. Parpinello, P. A. Kilmartin, A. Versari, *Appl. Spectrosc. Rev.* **2015**, *50*, 407.
- [41] F. S. Grasel, M. F. Ferrão, C. R. Wolf, *Spectrochim. Acta A Mol. Biomol. Spectrosc.* **2016**, *153*, 94.
- [42] A. Ricci, G. P. Parpinello, K. J. Olejar, P. A. Kilmartin, A. Versari, *Appl. Spectrosc. Rev.* **2015**, *69*, 1243.
- [43] G. Tondi, A. Petutschnigg, *Ind. Crop. Prod.* **2015**, *65*, 422.
- [44] M. Stratmann, B. der Bunsengesellschaft, *Phys. Chem. Chem. Phys.* **1990**, *94*, 626.
- [45] S. Yahya, A. M. Shah, A. A. Rahim, N. H. A. Aziz, R. Roslan, *J. Phys. Sci.* **2008**, *19*, 31.

How to cite this article: Bacca KRG, Lopes NF, Marcolino JB, dos Santos Grase F, da Costa EM. Performance of Quebracho extract as eco-friendly corrosion inhibitor for SAE 1010 steel in oil field environment. *Materials and Corrosion*. 2020;71: 155–165. <https://doi.org/10.1002/maco.201910963>